Probing interfacial effects with thermocapillary flows

M. Maza-Cuello,[1] C. Frétigny,[1] and L. Talini [2,*]

[1]*CNRS, Sciences et Ingénierie de la Matière Molle, ESPCI Paris, PSL Research University,
Sorbonne Université, 75005 Paris, France*
[2]*CNRS, Surface du Verre et Interfaces, Saint-Gobain, 93300 Aubervilliers, France*

We report on the thinning of supported liquid films driven by thermocapillarity. The liquids are oil films, of initial thicknesses of a few tens of microns. A local and moderate heating of the glass substrate on which they are spread induces a thermocapillary flow, which allows the formation of ultrathin films. We show that, within a given time range, the thinning dynamics of submicron-thick films is governed by the thermocapillary stress. It results in a simple dependency of the thickness profiles with time, which is evidenced by the collapse of the data onto a master curve. The master curve only depends on the liquid properties and on the thermal gradient, and allows a measurement of the latter. As the films further thin down to thicknesses within the range of molecular interactions, a deviation from the master curve appears. Although all investigated oils are supposedly fully wetting glass, the nature of the deviation differs between alkanes and silicone oils. We attribute the observed behaviors to differing signs of disjoining pressures, and this picture is confirmed by numerical resolution of the thin-film equation. We suggest thermocapillary flows can be used to finely probe molecular interactions.

I. INTRODUCTION

The surface tension of a pure liquid decreases with increasing temperature and a temperature gradient at its free surface results in a thermocapillary stress, inducing a flow away from the hottest region. The migration of liquids induced by a temperature gradient has been known and exploited for a long time [1]. It is used, for instance, for the patterning of surfaces, in the context of micromachining with molten metals [2,3]. In this process, a strong laser beam is shined on the surface of a body of metal, producing the melting of an upper layer which is driven mainly by the surface tension gradient. In recent years, a similar principle has been applied in the micropatterning of polymer melts for lithography techniques [4]. In contrast, in other applications thermocapillary flows may be undesired. For instance, they are known to cause failure of lubrication in tribo systems in which thermal gradients spontaneously appear; therefore, the design of devices must be thought in consequence [5]. From a more fundamental point of view, the behavior of a supported liquid film submitted to thermal gradients has been studied in different configurations. Theoretical works have focused on the dimpling of the free surface of the film that results from a thermocapillary stress, and to which both capillarity and gravity oppose [1,6–8]. Experimentally, controlled thermal gradients at the free surface can be created by locally heating the liquid by radiative transfer [9], but more usually it is the substrate they lie on that is heated. Focusing a laser at an absorbing substrate provides an easy way to locally increase its temperature and create a temperature gradient at a liquid interface by heat transfer [10–13]. Whatever the effect inducing the thermocapillary stress, the latter

---

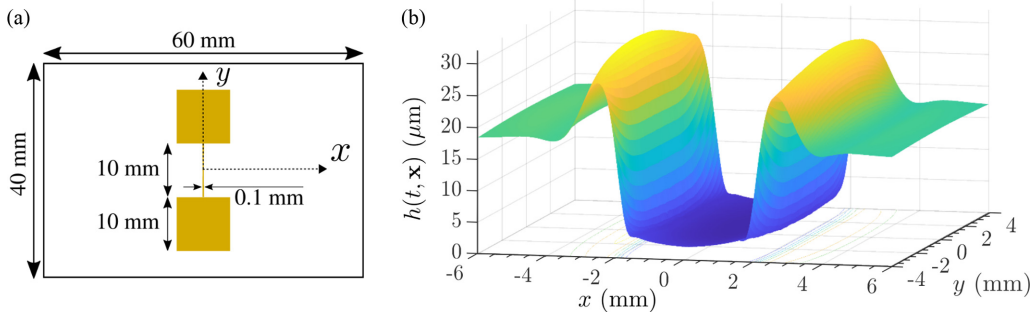*Corresponding author: laurence.talini@cnrs.fr

FIG. 1. (a) Top view of the glass substrate. On its bottom side, a microprinted circuit connected to a voltage generator creates the thermal gradient. (b) Typical thickness surface $h(t, \mathbf{x})$ at an intermediate stage of the dynamics, reconstructed surface via free-surface synthetic Schlieren method [14]. The thermocapillary effect promotes the apparition of a very thin ($h < 1\,\mu\text{m}$) layer that extends over several millimeters.

allows the formation and control of thin liquid films, in a region whose size is given by the extent of the thermal gradient [6]. Within this region, in which the films can reach submicron thicknesses even with a moderate temperature rise, intermolecular forces have nonnegligible effects, which, in particular, condition the rupture of the film. Thermocapillary-induced dewetting of liquids on solid substrates has thus been investigated by monitoring the thickness at the central hottest point [11,13]. However, to date, poor attention has been paid to the dynamics of the whole thin film region, in which intermolecular forces are large. Here, we show that interfacial effects at very small scales can be probed through accurate measurements of thickness variations in this region.

The paper is organized as follows. We describe the experimental setup and methods in Sec. II. A review of the hypotheses that are made leading to a well-known thin film equation describing the evolution of a thin liquid film under the action of thermocapillarity is discussed in Sec. III. We further present the experimental results in Sec. IV. Finally, Sec. V provides a conclusion and outlook for future work.

II. EXPERIMENTAL SETUP AND METHODS

A. Experimental setup

The liquid films are spread by spin coating on substrates that are rectangular glass slides of thickness $100\,\mu\text{m}$. Prior to deposition, the top side of the substrate is washed by spin coating isopropanol and acetone over it several times, finally letting it dry for a couple minutes before spreading the liquid. An electrical circuit is printed on the bottom side of the slides, with a pattern consisting of two squares connected by a line, as shown in Fig. 1(a). The squares are connected to a dc voltage generator and the resulting electrical current is measured. The central line, of width $100\,\mu\text{m}$, acts as a heat dissipator, generating a thermal field. We denote O the center of the line and Ox and Oy the axes, respectively, perpendicular and parallel to the line. We make the approximation that the induced thermal field does not depend on y, which is justified in the vicinity of the center of the line. We define the thermal excess $\theta(x) = T(x) - T_0$, where T_0 is the room temperature and $T(x)$ the thermal field. The dissipated power P along the line is a control parameter that sets the maximal temperature rise, $\theta_{\max} = \theta(0)$. In our experiments, $P \sim 1\,\text{mW}$ and $\theta_{\max} \sim 1\,\text{K}$. Infrared measurements have evidenced that the horizontal extent of the thermal gradient w is a few millimeters. The thermal gradient drives a flow in the liquid films away from the central line, inducing a thinning of the films along that line. A typical surface of a film once a very thin film has been formed at the central region is shown in Fig. 1(b). The profile was measured via an implementation of the free-surface synthetic Schlieren method [14], which we will not detail here since we focus on measurements at smaller thicknesses, which are described in the following. The

TABLE I. Investigated liquids with their main properties: viscosity, η, density, ρ, thermal coefficient of the surface tension, $\gamma_\theta = -\partial_T \gamma|_{T=T_0}$, and melting temperature, T_{melt}.

	η (mPas)	ρ (kg m^{-3})	γ_θ (N m^{-1} K^{-1})	T_{melt} (°C)	Ref.
Silicone oil	19	950	6.5×10^{-5}	< -40	[20,21]
n-C$_{16}$	2.2	733	8.7×10^{-5}	18	[16,22,23]
HMN	3.2	781	8.7×10^{-5}	-4	[17,22,24]

region we focus on is that at the center (where the heating line lies), which has been emptied of liquid so the thickness is below the micrometer scale in an area spanning several millimeters. We emphasize that, as expected, the measured profile only very weakly depends on y, which justifies the 1D profile we will consider in the following. Experiments were performed with different initial film thicknesses, h_0, and electrical powers P. The initial thickness h_0 is measured by optical profilometry just after spreading the films.

B. Investigated liquids

The investigated liquids are silicone oil (ABCR AB112154), n-hexadecane (Sigma-Aldrich), and a ramified isomer of hexadecane: 2,2,4,6,8,8-heptamethylnonane (HMN, Sigma-Aldrich). Their useful physical properties are listed in Table I; in particular, they have very close values of coefficient of surface tension variation, $\gamma_\theta = -\partial_T \gamma|_{T=T_0}$. In contrast, we emphasize that their melting temperatures are very different.

Since the temperature increase imposed to produce the thermocapillary effect remains modest, the variations of viscosity and density are small. An estimation from the thermal dependencies of these properties for the three liquids investigated [15–17] gives a variation on viscosity and density of around 2% and 0.1%, respectively, for a thermal rise of $\theta_{\text{max}} = 1$ K. Similarly, the variation of refractive index of alkanes [18] and silicone oil [19] caused by this temperature change is at most 0.01%. Therefore, the variations of viscosity, density, and refractive index produced by heating the liquid will be neglected in the following.

C. Thickness measurements

The thickness of the film at the central region, where it will be below the micrometer scale, is measured with three-color interferometry [25,26]. The measurement setup is sketched in Fig. 2(a). The cell is shined from below using a RGB-LED of peak wavelengths $\lambda_R = 635$ nm, $\lambda_G = 518$ nm, and $\lambda_B = 463$ nm. Images are taken from above with a CMOS monochrome camera. Images were taken typically each 10 min for silicone oil during a couple of days, and each 10 s during some hours for alkanes.

At any given measuring time, three images, one for each color, is taken. This leads to interference patterns such as the one shown in Fig. 2(b). From such an image, an interference profile $I_C(x)$ is obtained at each time and for each color $C = R$, G, B by averaging the intensity profiles along the y axis within a region spanning around 1 mm, which corresponds to the rectangle in Fig. 2(b). To obtain the thickness $h(x)$ from $I_C(x)$, one considers the theoretical linearized expression of transmission interference through a thin film of thickness h,

$$I_C^{\text{th}}(h) \propto 1 - A \cos\left(\frac{4\pi n h}{\lambda_C}\right),\tag{1}$$

where n is the refractive index of the liquid and A is a Fresnel coefficient depending on the refractive indexes of the media considered, in our experiments $A \simeq 0.012$. In the computations, the interference profiles $I_C(h)$ are convolved with a Gaussian function mimicking the broad-band emission of the LED source for each channel.
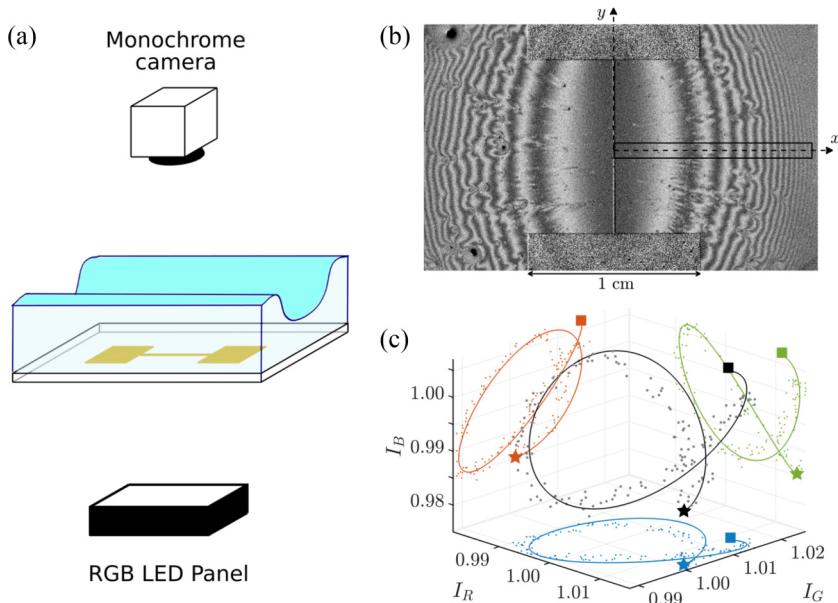
FIG. 2. (a) Sketch of the measurement setup. A RGB panel illuminates from below the experimental cell, consisting of a glass substrate over which a liquid film is deposited via spin coating. A monochrome camera on top takes pictures at specified intervals. (b) Typical interferometric profile of a silicone oil film obtained after an initial transient period. Here $\lambda_R = 635$ nm (red) and the height different between intensity maxima is $\Delta h = 113$ nm. The black rectangle indicates the region of interest for measuring the film dynamics, the interference intensity $I_R(x)$ is obtained by performing an average along the vertical direction (and similarly for green, I_G, and blue, I_B). (c) Grey dots: Interferometric data in intensity space (I_R, I_G, I_B) for the film at a given time. Black line: Theoretical intensity curve, with the thickness h as parameter. The colored points and lines are projections into the orthogonal planes for better visualization. Fitting the data points to the theoretical curve gives an absolute measurement of the thickness h at the corresponding x coordinate. The squares corresponds to $h = 80$ nm, the stars to $h = 300$ nm.

Working on the intensity space $\mathbf{I} = (I_R, I_G, I_B)$, as shown in Fig. 2(c), it is possible to use h as a fitting parameter of the theoretical curve for the data points, resulting in an absolute-thickness curve $h(x)$ at the time of measurement. This procedure allows us to obtain thicknesses below the first-order fringe, i.e., smaller than 100 nm, thus in the range where intermolecular forces are to be expected. In our current implementation, overall thickness profiles ranging from tens of nanometers to the micron scale can be measured with a nanometric accuracy. The floor sensitivity of the measurement is limited by experimental noise, which mainly originates from the camera sensor; as a result, thicknesses below 10 nm cannot be determined. Due to the opacity of the heating line, the film thickness cannot be measured for $|x| \lesssim 0.1$ mm.

D. Numerical integration

Numerical integration of the thin film equation discussed below is done using the `pdepe` numerical solver of MATLAB [27]. Since the equation is fourth order on the thickness gradient, the second derivative $u(t, x) \equiv \partial_x^2 h$ is considered as an independent field and a simple closure expression $u - \partial_x\{\partial_x h\} = 0$ is simultaneously solved. The initial condition is a film of homogeneous thickness, $h(0, x) = h_0$, $u(0, x) = 0$. For ease of convergence, the x spacing is logarithmic, allowing us to better describe the evolution close to the center as well as capturing the long-range evolution. The numerical integration typically lasted some hours.
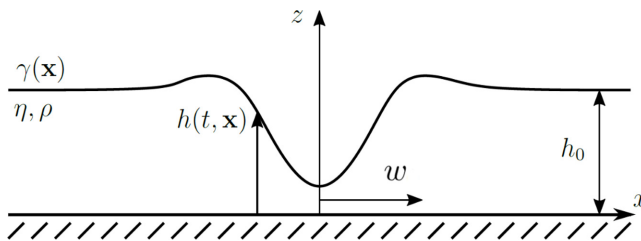
FIG. 3. Sketch of the film dynamics with main variables: A thin liquid film of density ρ and viscosity η, with initial thickness h_0, is deposited on top of a glass substrate which is heated locally, w being the decay length of the thermal field.

III. THEORETICAL BACKGROUND

As schemed in Fig. 3, we consider a homogeneous layer of incompressible liquid of constant viscosity η and density ρ with initial thickness h_0 that is submitted to a symmetric temperature excess $\theta(x)$. The excess temperature remains small: $\theta_{\max} = \theta(0) \ll T_0$, with T_0 the room temperature and all the properties of the liquid are assumed to be uniform. The resulting dynamics is assumed to be invariant along the y axis. In addition, since we use poorly volatile fluids, we consider that evaporation is negligible.

A. Hypotheses and dimensionless numbers

The order of magnitude of the thermocapillary stress is $\gamma_\theta \theta_{\max}/w \sim 0.1\,\text{Pa}$. The resulting velocity in a liquid film of thickness $10\,\mu\text{m}$ and viscosity $10^{-2}\,\text{Pa}\,\text{s}$ is $v \sim 100\,\mu\text{m}\,\text{s}^{-1}$. Since the liquids considered in the experiments have a thermal diffusivity $\kappa \sim 10^{-7}\,\text{m}^2\,\text{s}^{-1}$ [28,29], the thermal Péclet number $\text{Pe} = h_0 v/\kappa \sim 10^{-2}$ is small enough to consider thermal convection negligible. Therefore, the transport of heat from the substrate to the liquid is purely diffusive. In addition, the thermal field is established in a time $h_0^2/\kappa \sim 10^{-2}$ s, much faster than the timescale of hours involved in the dynamics. Hence, we assume that the thermal field is established instantaneously and that it is constant throughout the film's thickness. The Reynolds number $\text{Re} = h_0 v/\eta \sim 10^{-7}$ is also very small.

In the literature, a dimensionless number has been defined to measure the effect of the thermocapillary stress compared with that of hydrostatic pressure, $R = 3\Delta\gamma/2\rho g h_0^2$, where $\Delta\gamma = \gamma_\theta \theta_{\max}$ [6]. We typically work with $R \sim 10$, a larger thermocapillary effect than in Ref. [30] so the thickness at the center will always reach the region where intermolecular effects are relevant [6].

B. Thin-film equation

In experiments, the thermal field decays over a typical length $w \sim 2\,\text{mm}$ much larger than the initial thickness, $h_0 \ll w$, allowing us to consider a small gradient approximation. As a result, it is possible to obtain a lubrication approximation of the Navier-Stokes equations leading to a partial differential equation for the thickness profile $h(t, x)$ belonging to the family of thin film equations [31].

For the system defined by the conditions above and schematized in Fig. 3, the thin film equation reads [6]

$$\partial_t h + \frac{1}{3\eta}\partial_x\left\{h^3\partial_x\left[\gamma_0\partial_x^2 h - \rho g h + \Pi(h)\right]\right\} - \frac{\gamma_\theta}{2\eta}\partial_x\{h^2\partial_x\theta(x)\} = 0, \tag{2}$$

where the pressure contributions considered on the second term of the left-hand side are the capillary pressure, the hydrostatic pressure, and $\Pi(h)$ is a disjoining pressure term accounting for the intermolecular interactions. The third term represents the thermocapillary force driving film thinning.

Capillarity and gravity oppose film thinning whereas disjoining pressure may oppose or amplify thinning, according to its sign. The relative importance of the pressure terms vary as the film thins down, and this variation has been investigated theoretically [30]. If the initial thickness of the film is larger than the range of molecular interactions, then in a first stage the film dimples and both gravity and capillarity contribute to slow down its evolution. The central region of the film further empties and a central area of very small thickness is formed. In this region of small thickness and small curvature, both capillary and hydrostatic pressures are negligible. As a result, film thinning results from an interplay of thermocapillary stress and disjoining pressure. If the intermolecular forces are attractive, then spontaneous rupture of the film occurs. In the case of repulsive intermolecular forces, a fully equilibrated stationary state can be reached and has been observed in experiments [6,20]; it corresponds to a balance of the thermocapillary stress and disjoining pressure. In such a state, it would be possible, in principle, for the disjoining pressure to be measured if the thickness of the ultrathin liquid film at the central region is measured and the imposed thermal field is known. However, most experimental works have not aimed at measuring disjoining pressure and rather focused on the question of the film rupture [11,30]. In addition, an accurate determination of the thermal field is required to measure the disjoining pressure, which is a challenging task. In the geometry we investigate, the thermal gradients extend over millimetric lengths and we observe a very slow dynamics of the central region, which thins down during a timescale of days. In practice, this implies that the full equilibrium cannot be experimentally reached since other effects, such as sample contamination or liquid evaporation, appear at these very long timescales. Nevertheless, the thinning dynamics itself provides information on the intermolecular forces. Therefore, rather than trying to reach a stationary state, we take profit of the thinning dynamics to probe the intermolecular interactions at stake.

C. Pure thermocapillary regime

Before focusing on the effects of disjoining pressure, we first examine the preceding stage, in which the central area of small thickness has formed but its thickness is large enough for disjoining pressure to be neglected, i.e., larger than roughly 100 nm. In this stage, the capillary and gravitational pressures can as well be neglected in the description of the evolution, consistently with former works [6,30]. Film thinning is then entirely driven by thermocapillarity, which no effect opposes. Equation (2) then becomes

$$\partial_t h - \frac{\gamma_\theta}{2\eta} \partial_x \{h^2 \partial_x \theta(x)\} = 0. \tag{3}$$

Equation (3) can be solved by separation of variables, giving

$$h(t,x) = \frac{h_0}{1 + (t/t^*)} \frac{|\partial_x^2 \theta(0)|}{2\sqrt{|\partial_x \theta(x)|}} \int_0^x \frac{ds}{\sqrt{|\partial_s \theta(s)|}}, \tag{4}$$

where $t^* = 2\eta/(\gamma_\theta |\partial_x^2 \theta(0)| h_0)$. Since t^* is at most a few seconds and the timescale of the experiments is hours, the limit $t \gg t^*$ is quickly reached. Equation (4) then simplifies and the product $t \times h(t,x)$ can be expressed as

$$t \times h(t,x) = \frac{\eta}{\gamma_\theta} \frac{1}{\sqrt{|\partial_x \theta(x)|}} \int_0^x \frac{ds}{\sqrt{|\partial_s \theta(s)|}}. \tag{5}$$

The product $t \times h(t,x)$ is therefore independent of time and solely a function of the spatial coordinate, x. Since, in addition, it only depends on the liquid properties and not on the initial film thickness, for a given liquid, $t \times h(t,x)$ curves are expected to collapse onto a master curve that is a function of x only, whatever the initial conditions of the experiment. Inversely, at any given location x, the thickness has a simple dependency on time: $h(t,x) \propto t^{-1}$. This temporal scaling has been reported in experiments performed by heating a substrate with a laser beam [11]. The variations with time of the thickness of the oil film spread on the substrate were found to follow $h(t,0) \propto t^{-1}$
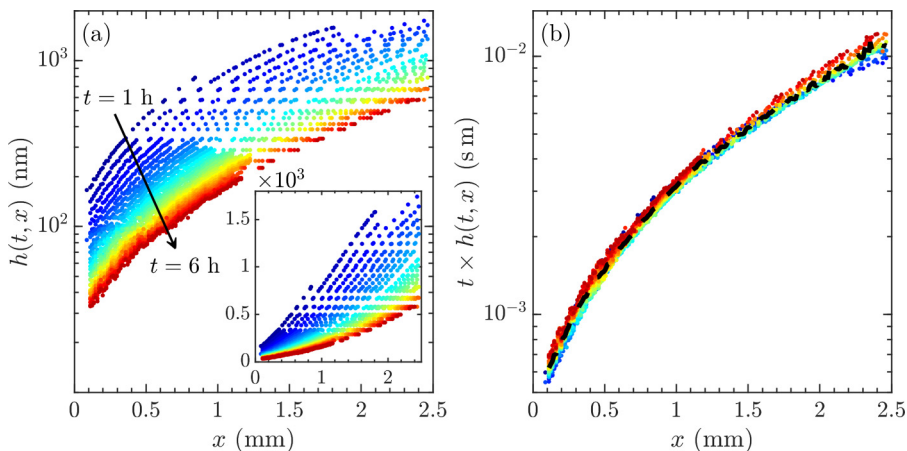
FIG. 4. (a) Experimental profiles of an experiment with silicone oil with $h_0 = 36 \pm 2\,\mu\text{m}$ and $P = 0.81(1)\,\text{mW}$. The time between profiles is 10 min. The inset shows the same profiles in linear scale. (b) The products $t \times h(t,x)$ for the experimental profiles of panel (a) at corresponding times collapse onto a master curve, which indicates that the local dynamics is solely described by the thermocapillary effect. The dashed line is the average of the experimental curves that is used to determine the thermal gradient.

for a wide range of laser power and beam waists under half a micrometer. It confirms the relevancy of a regime in which both capillarity and gravity are negligible. In the former work, the role of capillarity was found to be apparent only for very small beam waists at and below the micrometer scale, where the curvature of the film is sufficiently large. We demonstrate in the following that, in our experiments, capillarity and gravity are always negligible in the central area.

IV. EXPERIMENTAL RESULTS

A. Master evolution at intermediate thicknesses

In Fig. 4, we show the result of a typical measurement of the evolution at the central area, extending roughly a few millimeters away from the central line, similar to the one in Fig. 1(b). The evolution is displayed between 1 and 6 h after turning the thermal gradient on. Since the evolution is symmetric with respect to the origin of the x axis, the thickness of only one side of the film is reported. The experiment uses a film of silicone oil with initial thickness $h_0 = 36 \pm 2\,\mu\text{m}$ and the dissipated power is $P = 0.81(1)\,\text{mW}$.

The film thickness increases very slowly from the center to the edge: it reaches a few micrometers only over a distance of a few millimeters. The spatial variations of $t \times h(t,x)$ are also displayed in the figures: remarkably, all curves nicely collapse onto a master curve. According to the analysis of Sec. III, the collapse indicates that the effects of both capillary and hydrostatic pressures are negligible and that the dynamics is driven by thermocapillarity only, following the simple time dependency given by Eq. (5).

Following Eq. (5), the obtained master curve depends on the liquid properties, which are known, and on the thermal gradient driving the dynamics. The latter can hence be determined from the experimental master curve by inverting the relation given by Eq. (5) to get

$$\partial_x \theta(x) = -\frac{2\eta}{\gamma_\theta} \frac{1}{\langle t \times h(x,t)\rangle_{\exp}^2} \int_0^x \langle t \times h(s,t)\rangle_{\exp} ds. \tag{6}$$

where $\langle t \times h(x,t)\rangle_{\exp}$ is the experimentally determined master curve from the collapse of profiles as in Fig. 4(b), and is only a function of x. Figure 5 shows the thermal gradient $\partial_x \theta(x)$ obtained in this way. Since we do not have data up to $x = 0$, we extrapolate $\langle t \times h(x,t)\rangle_{\exp}$ by a constant for
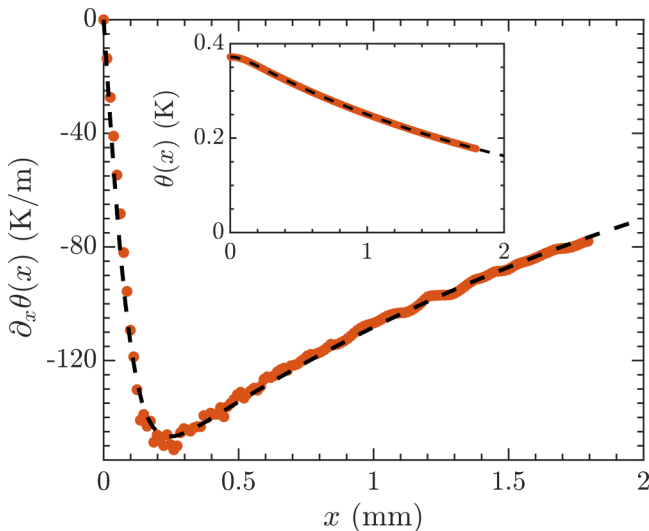
FIG. 5. Derivative of the thermal field $\partial_x\theta(x)$ obtained experimentally from the collapse of curves shown in Fig. 4(b) using Eq. (6). The dashed line represents a fit to the experimentally determined gradient following the derivative of the thermal excess given by Eq. (7) with the parameter values given in the text. Inset: Integrated thermal excess inferred from the experimentally determined gradient. The dashed line represents Eq. (7).

$x \leqslant 0.1$ mm to numerically compute the integral in Eq. (6). This extrapolation satisfies the symmetry requirement $\partial_x h(t, 0) = 0$ and we have checked that it results in a negligible correction for larger values of x. A heuristic expression for $\partial_x\theta(x)$ can further be determined from the temperature gradient found from the master curve. Once integrated, it corresponds to a thermal field given by

$$\theta(x) = \theta_{\max}\left[\operatorname{sech}\left(\frac{x}{\delta}\right)\right]^{\delta/w}, \tag{7}$$

where δ and w are two characteristic lengths. The length δ accounts for the finite length of the zone of maximum temperature. This length results from both the finite size of the central line of the circuit dissipating heat and the diffusion of heat through the thickness of the substrate. Since the line width and substrate thickness are both of $100\,\mu$m, δ is expected to be close to this value. The length w is the decay length of the thermal field at distances from the central line larger than δ and smaller than roughly 1 cm. We emphasize that at a longer range, the thermal excess is expected to go to zero asymptotically, with a characteristic decay length one order of magnitude larger than w. However, since we are interested in the central area of the film, for which submicron thicknesses are reached, Eq. (7) provides a satisfactory description of the thermal gradient in this area and further detail on the thermal field is not needed. In the particular case of Fig. 6, a fit of Eq. (7) to the experimentally determined gradient yields the following values: $\theta_{\max} = 0.37$ K, $\delta = 110\,\mu$m, and $w = 2.3$ mm. These values are consistent with independent measurements of the thermal field at the bare substrate measured with an IR camera. We emphasize that the modest value of $\theta_{\max}$ confirms that the liquids can be considered as having constant physical properties (i.e., viscosity, optical index, and density), although they are heated.

In summary, the master evolution followed by the film thickness within intermediate times allows the determination of the thermal gradient. The empirical expression that is obtained can be used in numerical resolutions to test the consistency of the results, as described in the next section.
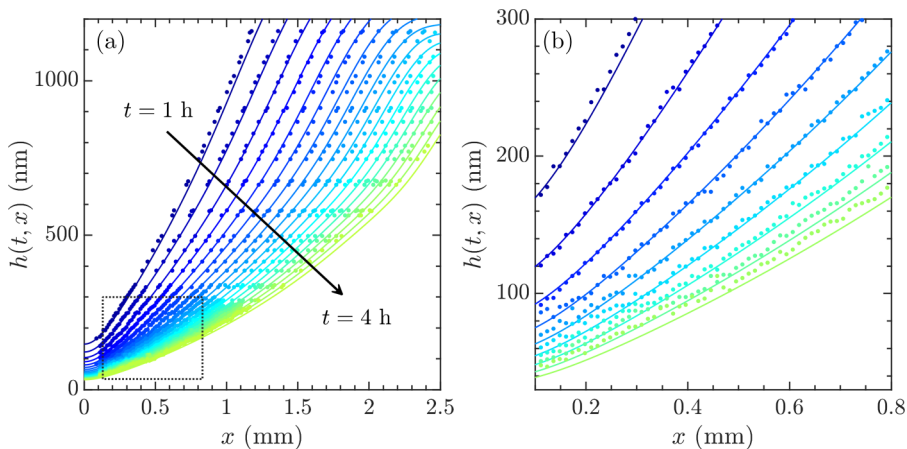
FIG. 6. (a) Same experimental thickness profiles as in Fig. 4. The solid lines were obtained by numerical integration of Eq. (2), with the thermal gradient of Fig. 5 and a zero disjoining pressure. (b) Zoomed view of the curves at small thicknesses showing the discrepancy between numerical and experimental data at this small scale (for better visualization, only one out of two curves is shown).

B. Comparison of experimental data with numerical resolution

Since the thermal field is determined, Eq. (2) that includes capillary and gravity terms can be solved, allowing the comparison of experimental data with numerical results obtained without any assumption. We emphasize that, in the following analysis, we do not consider the disjoining pressure term since we focus here on large thickness values for which intermolecular forces are negligible. In Fig. 6, we can see that the numerical integration faithfully represents the measured local dynamics, even for thicknesses well below the micron scale. Therefore, the determination of the thermal gradient based on the assumption of negligible effects of capillarity and gravity is fully validated.

As expected, at thicknesses below 100 nm, we observe that the numerical profiles deviate from experimental data. In this thickness range, both capillarity and gravity can still be neglected and the dynamics results from thermocapillary and intermolecular effects. We have not tried to quantitatively describe the disjoining pressure term in silicone oil. Instead, we focus on a qualitative effect resulting from intermolecular forces that we have evidenced.

C. Transition to the ultrathin film

We now examine the long-term regime, when the thickness is on the order of tens of nanometers, and when the effect of intermolecular forces becomes important. In this regime, the reduced thermocapillary evolution Eq. (4) is not valid anymore and the curves $t \times h(t, x)$ are expected to deviate from the master curve.

Figure 7 shows the long-term regime of the evolution when the thickness enters the range in which intermolecular forces are relevant, for the same experiment as Fig. 6. The corresponding $t \times h(t, x)$ curves clearly lie above the master curve, which demonstrates that the thinning induced by thermocapillarity has been slowed down. This deceleration can be explained by the presence of an effective repulsive intermolecular interaction that opposes the thermocapillary effect. A repulsion between the interfaces of the silicone oil film is expected since silicone oil totally wets the glass surface [32]. Therefore, the thinning slows down and the final stationary state would correspond to an equilibrium of disjoining pressure and thermocapillary stress.

We have performed similar experiments with alkanes, and Figs. 7(c) and 7(d) display the thickness profiles measured in a film of n-hexadecane. Because of the smaller viscosity of n-hexadecane,
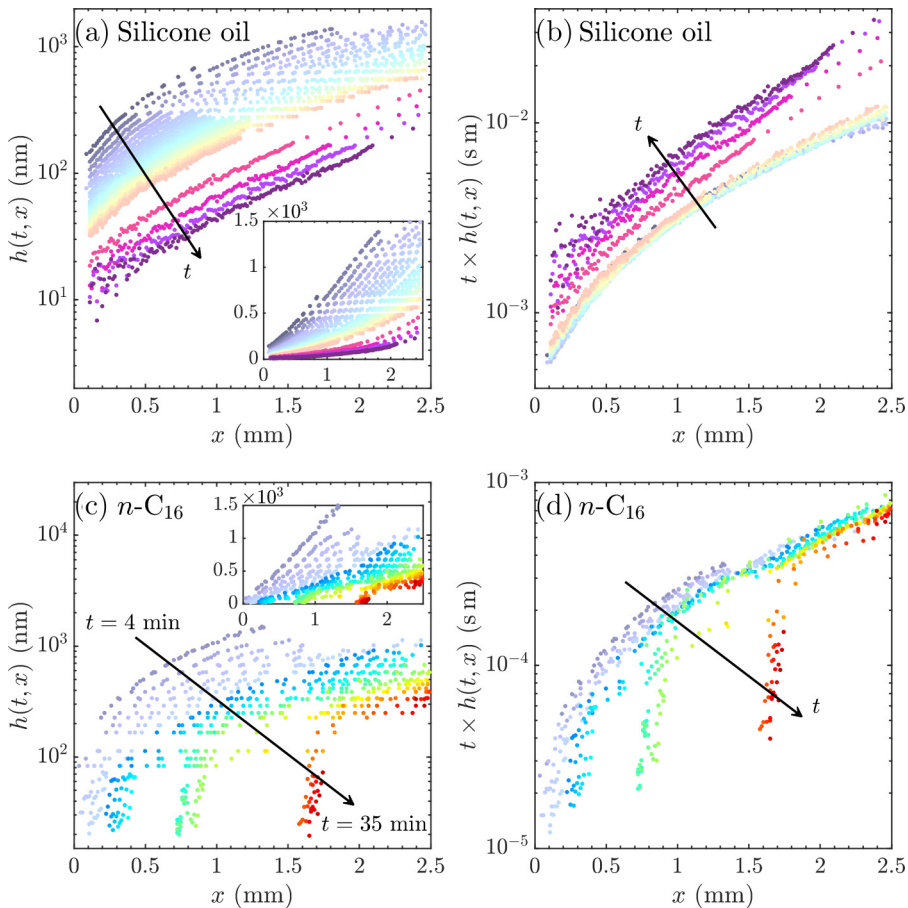
FIG. 7. (a), (b) Same plots as in Fig. 4 (dimmed curves), with the addition of profiles at later times $t = 13, 23, 33, 43$ h. The deviation of these last profiles from the master curve in panel (b) reveals the effect of intermolecular forces. (c) Experimental profiles $h(t, x)$ and (d) curves $t \times h(t, x)$ for an experiment using n-hexadecane (n-C$_{16}$), with $h_0 = 13.0(2)$ μm and $P = 0.95(9)$ mW. The time between profiles is 1 min. Observe that the time arrow in panel (d) points in the opposite direction of the corresponding arrow in panel (b).

the timescales of the experiment are much shorter. The curves at earlier times are nevertheless qualitatively similar to those of silicone oil and collapse as well onto a master curve. In contrast, at later times, the experimental profiles obtained with n-hexadecane reveal an acceleration of film thinning since they lie below the master curve. The acceleration is associated with an unstable behavior: the thickness profiles of n-hexadecane clearly collapse and form a foot receding from the center. We were, however, unable to evidence the presence or absence of an ultrathin film in the central region, since, if it exists, its thickness lies below the sensitivity level of the measurement (10 nm). We can nevertheless state that, in the range of investigated thicknesses, the disjoining pressure for n-hexadecane is attractive since it accelerates thinning instead of opposing it, in contrast to silicone oil.

This result is in contradiction with reports in the literature of hexadecane fully wetting glass surfaces [33], hence suggesting that the interactions between the interfaces of n-hexadecane films should be repulsive. The attractive interactions we evidence rather evoke a partial or pseudopartial wetting of n-hexadecane on glass. In the case of partial wetting, the spreading parameter is negative and the equilibrium situation is a drop sitting on the substrate with a finite angle of the contact line;
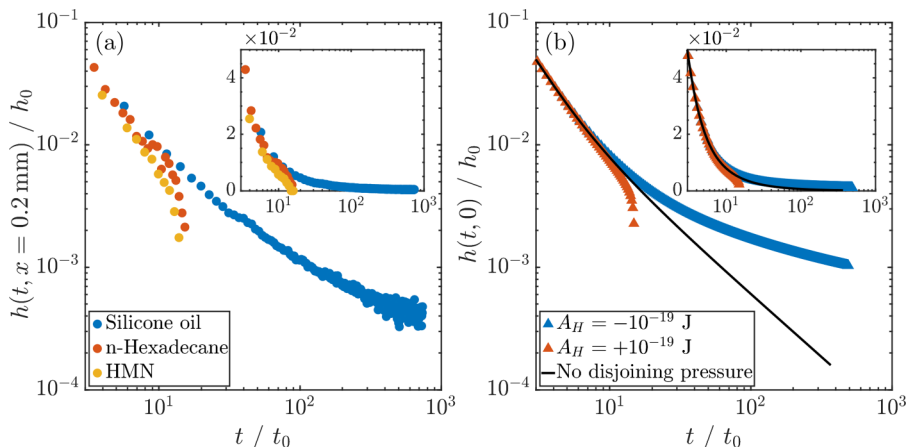
FIG. 8. (a) Comparison of the thickness evolution near the center, $h_c(t) = h(t, x = 0.2\,\text{mm})$, for the experiment with silicone oil and with n-hexadecane of Fig. 7. The time has been scaled by a thermocapillary timescale $t_0 = 2\eta w^2/(\Delta\gamma h_0)$ and the thickness by h_0. Silicone oil: $h_0 = 36 \pm 2\,\mu\text{m}$, $\theta_{\max} = 0.37\,\text{K}$, $w = 2.3\,\text{mm}$ ($t_0 \simeq 211\,\text{s}$). n-hexadecane: $h_0 = 13.0(2)\,\mu\text{m}$, $\theta_{\max} = 0.44\,\text{K}$, $w = 2.2\,\text{mm}$ ($t_0 \simeq 42\,\text{s}$). HMN: $h_0 = 19.5(6)\,\mu\text{m}$, $\theta_{\max} = 0.54\,\text{K}$, $w = 2.2\,\text{mm}$ ($t_0 \simeq 30\,\text{s}$). (b) Same as in (a) but with profiles at the center $h(t, 0)$ from the numerical integration of Eq. (2) with physical properties of n-hexadecane, when the intermolecular forces generate an effective repulsion ($A_H < 0$) versus attraction ($A_H > 0$) of the interfaces. In the case where there is no disjoining pressure (e.g., $A_H = 0$), the evolution follows Eq. (4), i.e., $t \times h(t, 0) \propto \text{const}$ for $t \gg t_0$.

in the case of pseudopartial wetting, the spreading parameter is positive and the equilibrium situation is also a drop with a finite angle but that sits on a film of nanometric thickness. The latter situation results from nonmonotonic variations of the disjoining pressure with thickness [32]. Since glass is a material of high surface energy, it is likely that the spreading parameter is positive, favoring the hypothesis of pseudopartial wetting.

We emphasize that we observe the same unexpected behavior with the ramified alkane HMN as with the linear n-hexadecane, and hence that it does not result from crystallisation effects. Actually, it is well-known that surface freezing occurs in alkanes at temperatures up to 3 K above their solidification temperature [34], which affects the wetting behavior of n-hexadecane films [35,36]. However, HMN has a crystallization temperature which is well below room temperature and remains liquid at room temperature even when present on subnanometric layers [37]. As a result, surface freezing cannot be invoked to explain the observed behaviors that are common to n-hexadecane and HMN. We rather suggest that these alkanes only pseudopartially wet glass. In this case, the distinction from total wetting is difficult in macroscopic experiments if the equilibrium angles are small. In addition, times to attain an equilibrium state may reach the scale of the week [38]. These difficulties are likely to explain why n-hexadecane has been suggested to totally wet glass, and show that static experiments at the macroscopic scale may not be sufficient to determine wetting behaviors properly.

Additional insight is provided by numerical integration of the thin-film equation with a given disjoining pressure. In the apolar liquids and the range of film thicknesses we investigate, intermolecular forces are expected to be nonretarded van der Waals interactions $\Pi(h) = -A_H/(6\pi h^3)$, where A_H is the Hamaker constant [39]. A repulsive interaction then corresponds to a negative Hamaker constant and an attraction to a positive Hamaker constant. Using typical values for the thermal gradient, we have solved Eq. (2) with disjoining pressure terms of, respectively, attractive and repulsive nature. Because of numerical instabilities, full spatial variations as in Fig. 7 cannot be obtained in the case of attractive intermolecular forces. We nonetheless show in Fig. 8 the dynamics

at the center, $h(t, 0)$, for attractive ($A_H > 0$) and repulsive ($A_H < 0$) interactions, as well as for zero disjoining pressure. Since the dynamics at the center cannot be measured in the experiment, the dynamics measured at a distance of 0.2 mm from the center $h(t, x = 0.2\,\text{mm})$ is displayed for experiments with silicone oil and both n-hexadecane and HMN. To compare the dynamics measured in different experimental conditions with liquids that have different viscosities, we have represented the dimensionless thickness a function of the ratio of the time and a thermocapillary timescale, $t_0 = 2\eta w^2/(\Delta\gamma h_0)$. As expected, the case $A_H = 0$ results in a pure-thermocapillary evolution $h(t, 0) \propto t^{-1}$. In contrast, for nonzero interactions, a deviation from t^{-1} variations appears for thicknesses in the range of tens on nanometers. For $A_H < 0$, the thinning is slowed down, whereas for $A_H > 0$ it is abruptly accelerated, leading to film rupture. Changing the sign of the disjoining pressure in the equation therefore satisfactorily accounts for the different behaviors observed. This result confirms that attractive intermolecular forces, at least in the thickness range investigated, are at stake between the interfaces of films of the considered alkanes. Beyond this qualitative finding, the very similar shape of the experimental and computed curves suggest that the expression for disjoining pressure we use is close to the real one. However, we have found that the dynamics in silicone oil could not be quantitatively described by the simple law we have used: Clearly, in Fig. 8 the experimental thinning is faster than in the computation. Consistently, the full thickness profiles, as the ones reported in Fig. 6 could not be described, even when changing the value of the Hamaker constant. This discrepancy may result from the fact that the used silicone oil is not monodisperse but rather constituted by a mixture of macromolecules of different lengths. Mixture effects have actually been predicted to change the exponent of the thickness dependency of molecular interactions [40]. These complex effects are out of the scope of the present paper and we have not tried to further determine the disjoining pressure at stake. However, since silicone oil is widely used as a model wetting liquid, it could be an interesting aim for future research.

V. CONCLUSION

In conclusion, we have demonstrated that the dynamics of thin films induced by a thermal gradient can serve as a tool for investigating intermolecular forces. We predict and experimentally evidence a regime in which thermocapillarity fully drives thinning. The thermal gradient can thus be determined from thickness profile measurements and, in turn, be used to compute the expected dynamics when intermolecular forces are at stake. We demonstrate that thickness measurements allow a clear discrimination between the cases of attractive and repulsive interactions between the interfaces of the liquid films. The experiments reveal an unexpected behavior of both linear and ramified alkanes when film thicknesses reach a few tens of nanometers, and thus show that accurate probes of liquid films at very small scales are still needed.

ACKNOWLEDGMENTS

[1] A. V. Hershey, Ridges in a liquid surface due to the temperature dependence of surface tension, Phys. Rev. 56, 204 (1939).

[2] T. R. Anthony and H. E. Cline, Surface rippling induced by surface-tension gradients during laser surface melting and alloying, J. Appl. Phys. 48, 3888 (1977).

[3] D. A. Willis and X. Xu, Transport phenomena and droplet formation during pulsed laser interaction with thin films, J. Heat Transfer 122, 763 (2000).

[4] J. P. Singer, Thermocapillary approaches to the deliberate patterning of polymers, J. Polym. Sci., Part B: Polym. Phys. 55, 1649 (2017).

[5] Q. Dai, W. Huang, X. Wang, and M. Khonsari, Directional interfacial motion of liquids: Fundamentals, evaluations, and manipulation strategies, Tribol. Int. **154**, 106749 (2021).

[6] M. J. Tan, S. G. Bankoff, and S. H. Davis, Steady thermocapillary flows of thin liquid layers. I. Theory, Phys. Fluids **2**, 313 (1990).

[7] S. M. Pimputkar and S. Ostrach, Transient thermocapillary flow in thin liquid layers, Phys. Fluids **23**, 1281 (1980).

[8] L. Y. Yeo, R. V. Craster, and O. K. Matar, Marangoni instability of a thin liquid film resting on a locally heated horizontal wall, Phys. Rev. E **67**, 056315 (2003).

[9] D. L. Hitt and M. K. Smith, Radiation-driven thermocapillary flows in optically thick liquid films, Phys. Fluids **5**, 2624 (1993).

[10] H. Chraïbi and J.-P. Delville, Thermocapillary flows and interface deformations produced by localized laser heating in confined environment, Phys. Fluids **24**, 032102 (2012).

[11] H. M. J. M. Wedershoven, C. W. J. Berendsen, J. C. H. Zeegers, and A. A. Darhuber, Infrared laser induced rupture of thin liquid films on stationary substrates, Appl. Phys. Lett. **104**, 054101 (2014).

[12] B. Pottier, C. Fretigny, and L. Talini, Boundary Condition in Liquid Thin Films Revealed Through the Thermal Fluctuations of Their Free Surfaces, Phys. Rev. Lett. **114**, 227801 (2015).

[13] D. S. Klyuev, V. M. Fliagin, S. V. Semenov, and N. A. Ivanova, Thermocapillary deformation induced by laser heating of thin liquid layers: Physical and numerical experiments, Int. J. Heat Mass Transf. **172**, 121020 (2021).

[14] F. Moisy, M. Rabaud, and K. Salsac, A synthetic schlieren method for the measurement of the topography of a liquid interface, Exp. Fluids **46**, 1021 (2009).

[15] C. C. Roberts, A. Graham, M. Nemer, L. M. Phinney, R. M. Garcia, M. M. Soehnel, and E. K. Stirrup, Physical properties of low-molecular weight polydimethylsiloxane fluids, Technical Report No. SAND2017-1242 (Sandia National Laboratories, USA, 2017), https://www.osti.gov/servlets/purl/1343365.

[16] G. P. Dubey and M. Sharma, Temperature and composition dependence of the densities, viscosities, and speeds of sound of binary liquid mixtures of 1-butanol with hexadecane and squalane, J. Chem. Eng. Data **53**, 1032 (2008).

[17] D. J. Luning Prak, S. M. Alexandre, J. S. Cowart, and P. C. Trulove, Density, viscosity, speed of sound, bulk modulus, surface tension, and flash point of binary mixtures of *n*-dodecane with 2,2,4,6,6-pentamethylheptane or 2,2,4,4,6,8,8-heptamethylnonane, J. Chem. Eng. Data **59**, 1334 (2014).

[18] D. L. Camin, A. F. Forziati, and F. D. Rossini, Physical properties of n-hexadecane, n-decylcyclopentane, n-decylcyclohexane, 1-hexadecene and n-decylbenzene, J. Phys. Chem. **58**, 440 (1954).

[19] T. L. Van Raalte, Measurement of the refractive index of silicone oils for the UKAEA, J. Opt. Soc. Am. **50**, 85_2 (1960).

[20] C. Clavaud, M. Maza-Cuello, C. Frétigny, L. Talini, and T. Bickel, Modification of the Fluctuation Dynamics of Ultrathin Wetting Films, Phys. Rev. Lett. **126**, 228004 (2021).

[21] E. Ricci, R. Sangiorgi, and A. Passerone, Density and surface tension of dioctylphthalate, silicone oil and their solutions, Surf. Coat. Technol. **28**, 215 (1986).

[22] G. Korosi and E. S. Kovats, Density and surface tension of 83 organic liquids, J. Chem. Eng. Data **26**, 323 (1981).

[23] B. M. Ocko, X. Z. Wu, E. B. Sirota, S. K. Sinha, O. Gang, and M. Deutsch, Surface freezing in chain molecules: Normal alkanes, Phys. Rev. E **55**, 3164 (1997).

[24] Chemical Book, 2,2,4,4,6,8,8-heptamethylnonane technical information.

[25] J. Schilling, K. Sengupta, S. Goennenwein, A. R. Bausch, and E. Sackmann, Absolute interfacial distance measurements by dual-wavelength reflection interference contrast microscopy, Phys. Rev. E **69**, 021901 (2004).

[26] J. de Ruiter, F. Mugele, and D. van den Ende, Air cushioning in droplet impact. I. Dynamics of thin films studied by dual wavelength reflection interference microscopy, Phys. Fluids **27**, 012104 (2015).

[27] See https://www.mathworks.com/help/matlab/ref/pdepe.html for the documentation page of pdepe. Run with MATLAB R2022a.

[28] Bluestar Silicones, Rhodorsil Oils 47 technical information, 2021.

[29] C. Vélez, M. Khayet, and J. M. Ortiz de Zárate, Temperature-dependent thermal properties of solid/liquid phase change even-numbered n-alkanes: n-Hexadecane, n-octadecane and n-eicosane, Appl. Energy **143**, 383 (2015).

[30] J. P. Burelbach, S. G. Bankoff, and S. H. Davis, Steady thermocapillary flows of thin liquid layers. II. Experiment, Phys. Fluids **2**, 322 (1990).

[31] A. Oron, S. H. Davis, and S. G. Bankoff, Long-scale evolution of thin liquid films, Rev. Mod. Phys. **69**, 931 (1997).

[32] P.-G. De Gennes and F. Brochard-Wyart, *Gouttes, Bulles, Perles et Ondes* (Belin Éducation, Paris, France, 2015).

[33] S. Shiri, S. Sinha, D. A. Baumgartner, and N. J. Cira, Thermal Marangoni Flow Impacts the Shape of Single Component Volatile Droplets on Thin, Completely Wetting Substrates, Phys. Rev. Lett. **127**, 024502 (2021).

[34] X. Z. Wu, E. B. Sirota, S. K. Sinha, B. M. Ocko, and M. Deutsch, Surface Crystallization of Liquid Normal-Alkanes, Phys. Rev. Lett. **70**, 958 (1993).

[35] P. Lazar, H. Schollmeyer, and H. Riegler, Spreading and Two-Dimensional Mobility of Long-Chain Alkanes at Solid/Gas Interfaces, Phys. Rev. Lett. **94**, 116101 (2005).

[36] L. Lu, K. J. Zander, and Y. Cai, Stability of the parallel layer during alkane spreading and the domain structures of the standing-up layer, Langmuir **26**, 5624 (2010).

[37] N. N. Gosvami, S. K. Sinha, and S. J. O'Shea, Squeeze-Out of Branched Alkanes on Graphite, Phys. Rev. Lett. **100**, 076101 (2008).

[38] E. Pérez, E. Schäffer, and U. Steiner, Spreading dynamics of polydimethylsiloxane drops: Crossover from laplace to van der Waals spreading, J. Colloid Interface Sci. **234**, 178 (2001).

[39] N. V. Churaev, Surface forces in wetting films, Colloid J. **65**, 263 (2003).

[40] B. Derjaguin and N. Churaev, On the question of determining the concept of disjoining pressure and its role in the equilibrium and flow of thin films, J. Colloid Interface Sci. **66**, 389 (1978).